Supporting information of

Warming shifts surface ozone peak to higher temperatures

Haolin Wang[1,2,3,6], Shuai Li[1,3], Haofan Wang[1,3], Funing Li[4], Aiguo Dai[5], Arlene M. Fiore[4], Paul I. Palmer[6,7], Drew T. Shindell[8], Seok-Woo Son[9], Haichao Wang[1,3], Kai Wu[10], Ke Li[11], Shaojia Fan[1,3], Gregory R. Carmichael[12], Xiao Lu[1,3*], Meng Gao[2*]

[1] School of Atmospheric Sciences, Sun Yat-sen University, and Southern Marine Science and Engineering Guangdong Laboratory (Zhuhai), Zhuhai, Guangdong, China

[2] Department of Geography, Hong Kong Baptist University, Hong Kong, China

[3] Guangdong Provincial Observation and Research Station for Climate Environment and Air Quality Change in the Pearl River Estuary, Zhuhai, Guangdong, China

[4] Department of Earth, Atmospheric, and Planetary Sciences, Massachusetts Institute of Technology, Cambridge, MA, USA.

[5] Department of Atmospheric and Environmental Sciences, University at Albany, State University of New York, Albany, NY, USA

[6] School of GeoSciences, University of Edinburgh, Edinburgh, United Kingdom

[7] National Centre for Earth Observation, University of Edinburgh, Edinburgh, United Kingdom

[8] Nicholas School of the Environment, Duke University, Durham, NC, USA

[9] School of Earth and Environmental Sciences, Seoul National University, Seoul, Republic of Korea

[10] Department of Civil and Environmental Engineering, University of California, Irvine, CA, USA

[11] State Key Laboratory of Climate System Prediction and Risk Management/Joint International Research Laboratory of Climate and Environment Change, School of Environmental Science and Engineering, Nanjing University of Information Science & Technology, Nanjing, China

[12] College of Engineering, University of Iowa, Iowa City, IA, USA

Correspondence: Xiao Lu (luxiao25@mail.sysu.edu.cn) and Meng Gao (mmgao2@hkbu.edu.hk)

Contents

Supplementary Text S1-S2
Supplementary Figures S1-S18
Supplementary Tables S1-S3
References

Supplementary Text S1 | Data description

Nationwide hourly measurements of ground-level ozone and CO from ~2000 urban monitoring stations across China for 2015–2019 were obtained from the China National Environmental Monitoring Center (CNEMC). Concurrent hourly ozone and CO measurements for 2015–2019 in Europe and 1980-2022 in the United States were sourced from the European Environment Agency (EEA) and the EPA Air Quality System (AQS), respectively, while data for South Korea (2015-2019) and Japan (1980-2022) were obtained from the Korean Ministry of Environment and the National Institute for Environmental Studies. We performed data quality control on the hourly surface data by following our previous guidelines to exclude unreliable data outliers[1]. A minimum of 18 valid hourly observations per day was required to ensure robust calculation of the daily maximum 1-hour average (MDA1) ozone. Only sites with valid ozone data for at least 60% of summer days (≥276 of 460 days) were included to derive a robust ozone-temperature relationship. To facilitate a consistent analysis of inter-species co-variations, only sites with collocated and temporally matched CO and ozone measurements were selected for Figure S14, including 1,397 sites in China, 55 in Japan, 310 in South Korea, 552 in Europe, and 194 in the United States.

Supplementary Text S2 | Comparison of methods for estimating the cut-off temperature of ozone suppression

Some previous studies identified “ozone suppression” at high temperatures, based on changes in ozone-temperature slopes across different temperature bins[2-4]. For example, Steiner et al. (2010) defined ozone suppression using a one-tailed Z test to evaluate if $m_{O3\text{-}T}$ within an “extremely high” temperature regime is significantly less than that within a “normal” temperature regime at a 95% confidence level[2]. The “cutoff temperature” is defined as the temperature resulting in the most significantly different $m_{O3\text{-}T}$ between the normal temperature and the extremely high temperature slopes. While both our study and previous work address the suppression of ozone increases at extreme temperatures, the goals and methods are different. “Suppression” defined in previous studies includes both a deceleration in the rate of ozone increase and a complete reversal (*i.e.*, a transition from increase to decrease) with increasing temperature. In contrast, our study focuses exclusively on the reversal of ozone-temperature relationship. Our study aims to explicitly identify the temperature hosting the highest ozone concentrations, as these extreme levels pose the greatest risks to air quality and public health. Consequently, the corresponding reversal temperature (*i.e.*, peak-ozone temperature) serves as the key metric. Although our definition of ozone-temperature relationship reversal (described in Methods) does not rely on statistical tests, the robustness of our approach is ensured by using a 5-year observation window, and by excluding temperature bins with insufficient records.

Figure S2 exemplifies the difference between the two methods. At two selected sites in China, we can identify ozone peaks at a specific temperature bin (305K for site 1880A and 308K for site 2478A, defined as peak-ozone temperature), beyond which ozone concentrations decrease. This pattern demonstrates a clear reversal in the ozone-temperature relationship. Investigating the drivers behind the decrease from these peak temperatures is the primary focus of our study. However, neither site is classified as exhibiting “ozone suppression” based on the Z-test. This is because ozone observations beyond the peak temperature are typically sparse (often fewer than 100 data points), in sharp contrast to the thousands of observations available within the normal temperature range. This imbalance in sample size limits the statistical power required to pass the Z-test, potentially resulting in the loss of valuable samples for analyzing ozone responses at high temperatures.

We evaluated the sensitivity of the diagnosed peak-ozone temperature to the choice of ozone percentiles (75th, 85th, and 95th) within each temperature bin, and compared these results with the “cutoff temperature” determined by the Z-test approach for identifying “ozone suppression” (Fig. S3). Overall, the probability density functions of peak-ozone temperatures derived from different percentiles remain largely consistent, with regional mean differences of less than 0.8 K. However, utilizing lower ozone percentiles reduces the number of sites identified as exhibiting an ozone-temperature reversal. The proportion of sites classified as showing “ozone suppression” via the Z-test ranges from 38.1% to 49.3% across the five regions, consistent with previous studies in China[4]. Notably, more than 68% of the sites identified by the Z-test are also captured by our method for detecting ozone-temperature reversal, despite the differing objectives of the two approaches. The derived 'cutoff' temperatures are similar to the peak-ozone temperatures in China but show larger discrepancies in the other regions.

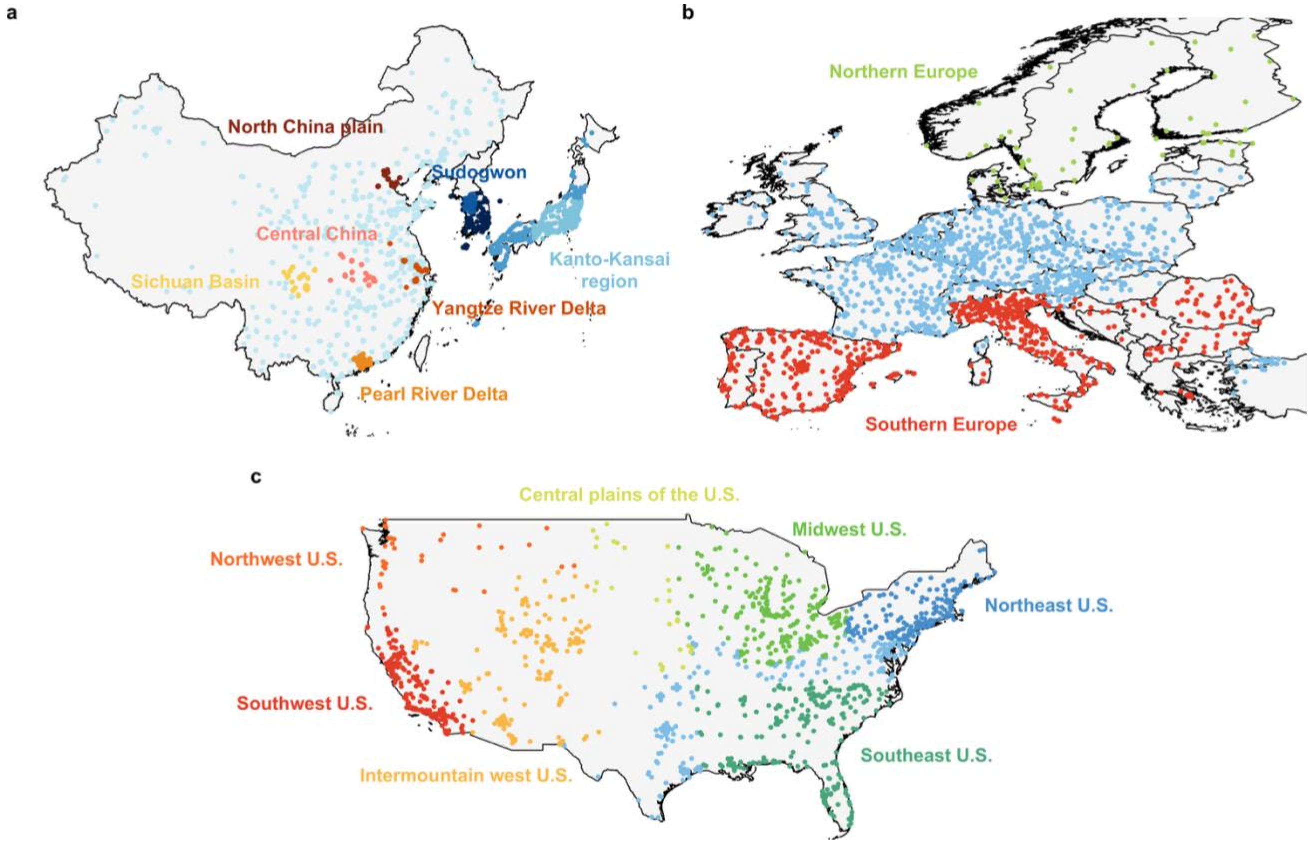

Supplementary Figure S1 | Locations of ozone monitoring sites over 2015–2019 used in this study.

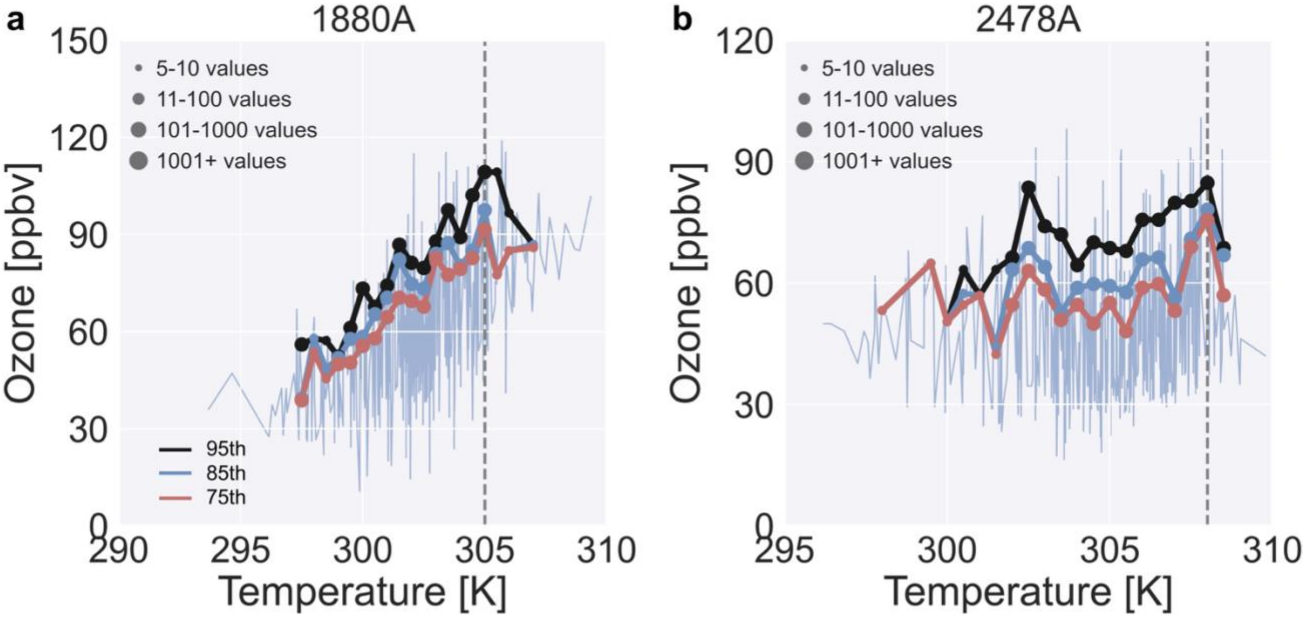

Supplementary Figure S2 | Examples of sites exhibiting ozone-temperature relationship reversal not captured by the Z-test method. Ozone–temperature relationships at two sites in China are shown. The colored lines indicate the 95th, 85th, and 75th percentiles of ozone within each bin (0.5K intervals). Vertical grey dashed lines indicate the peak-ozone temperature. Despite displaying a clear ozone-temperature relationship reversal, these sites were not identified as significant by the Z-test method[2-4].

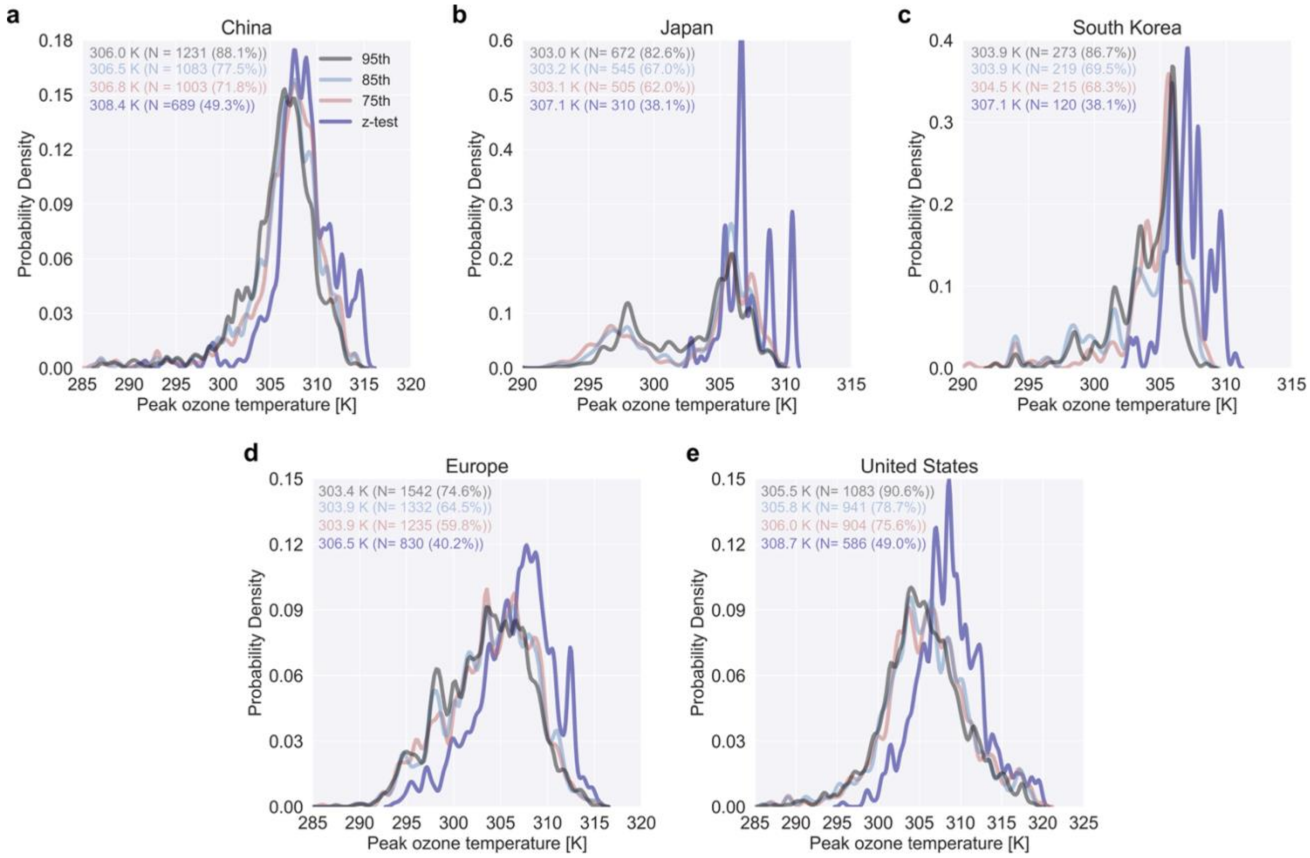

Supplementary Figure S3 | Comparison of peak-ozone temperature distributions derived from different percentiles at each temperature bins with the cutoff temperature derived from the Z-test approach. Probability density functions of temperature for five regions—China (CHN), Japan (JP), South Korea (Kr), Europe (EU), and the United States (US) are shown. The texts in each panel list the regional mean peak-ozone temperature or cutoff temperature, the number of valid sites, and the proportion of sites relative to the total.

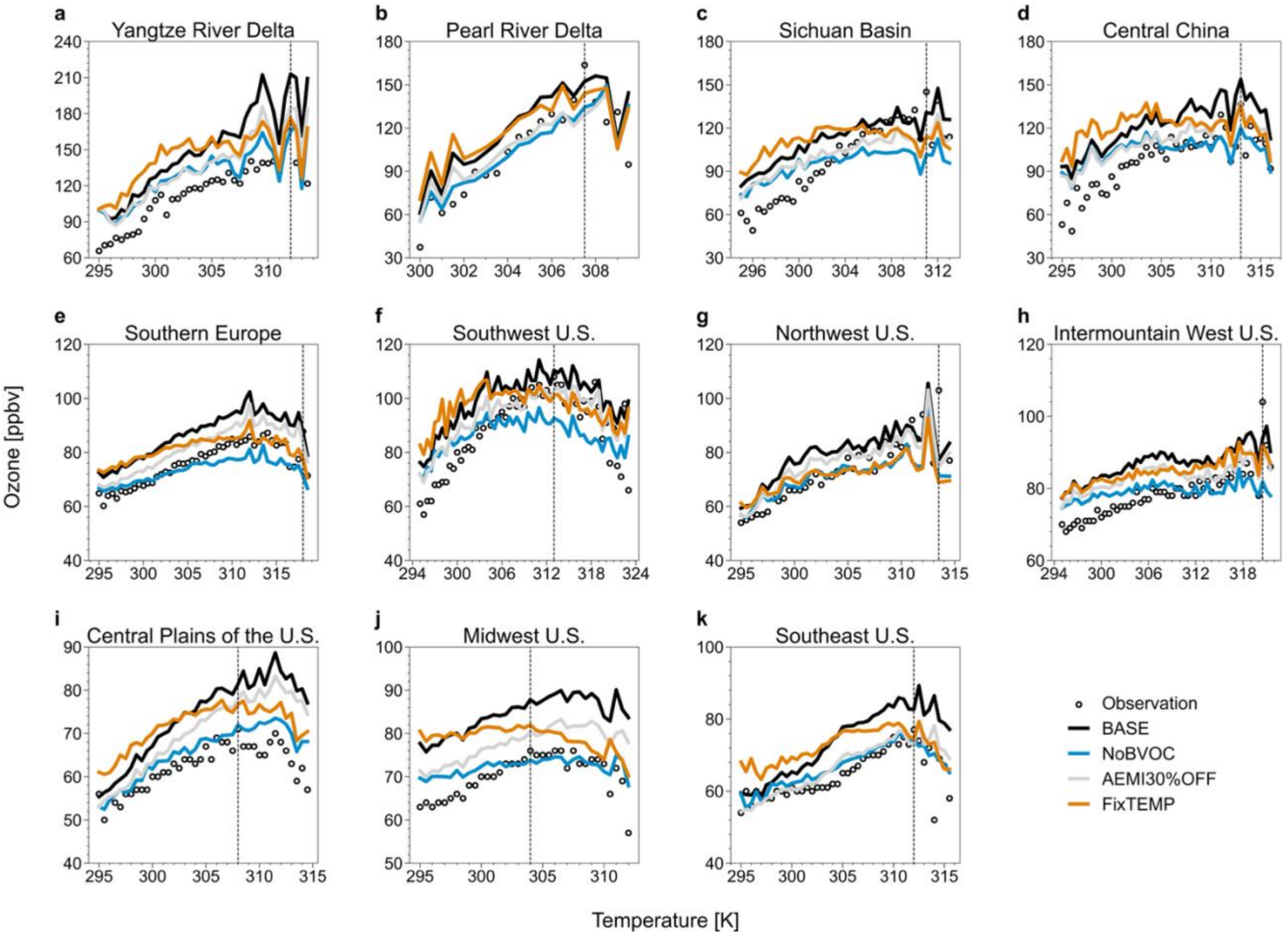

Supplementary Figure S4 | Same as Figure 2a but for key regions within China, Europe, and the United States.

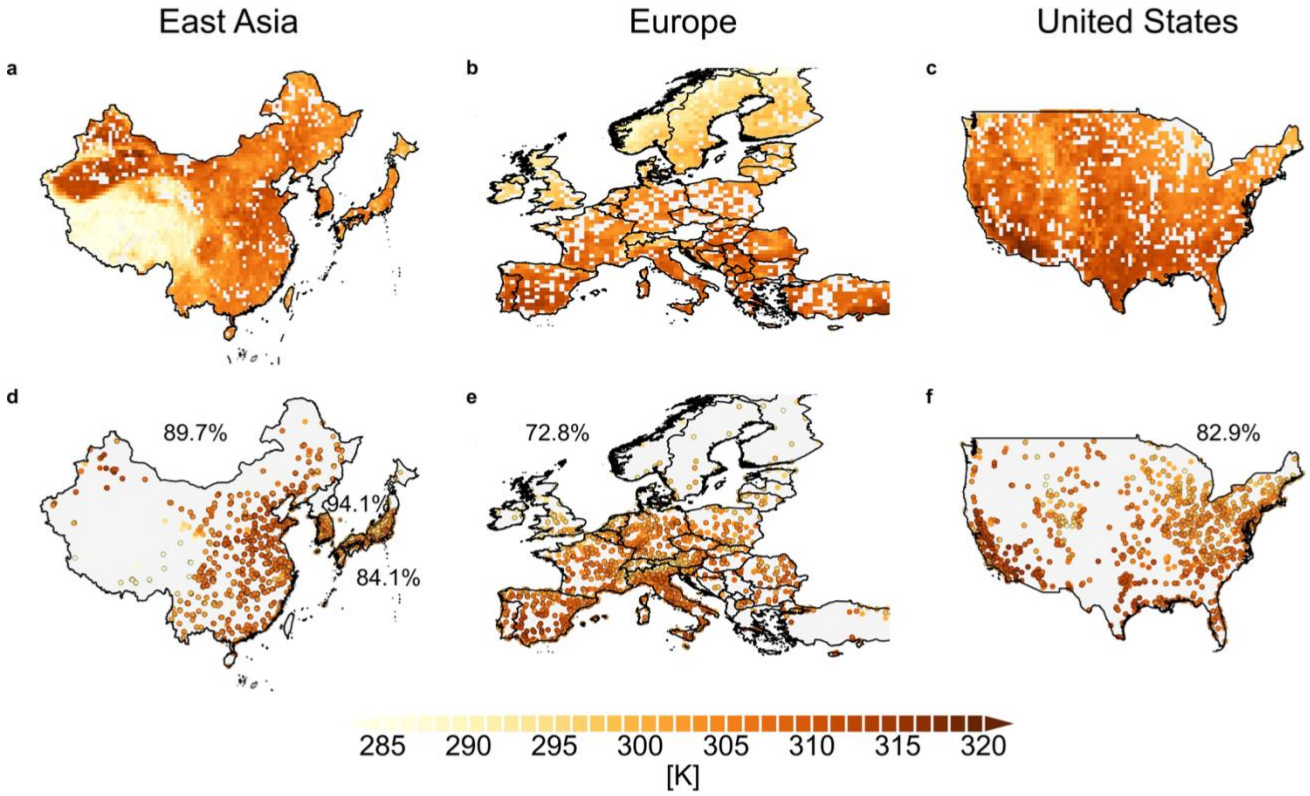

Supplementary Figure S5 | GEOS-Chem simulated and observed peak-ozone temperatures across East Asia, Europe, and the United States. The first row shows simulated results, and the second row shows observed results. Circles with black edges indicate sites where the model captures observed ozone-temperature reversal. The percentage of sites within each region where the model captures the observed ozone-temperature reversal is shown as an inset.

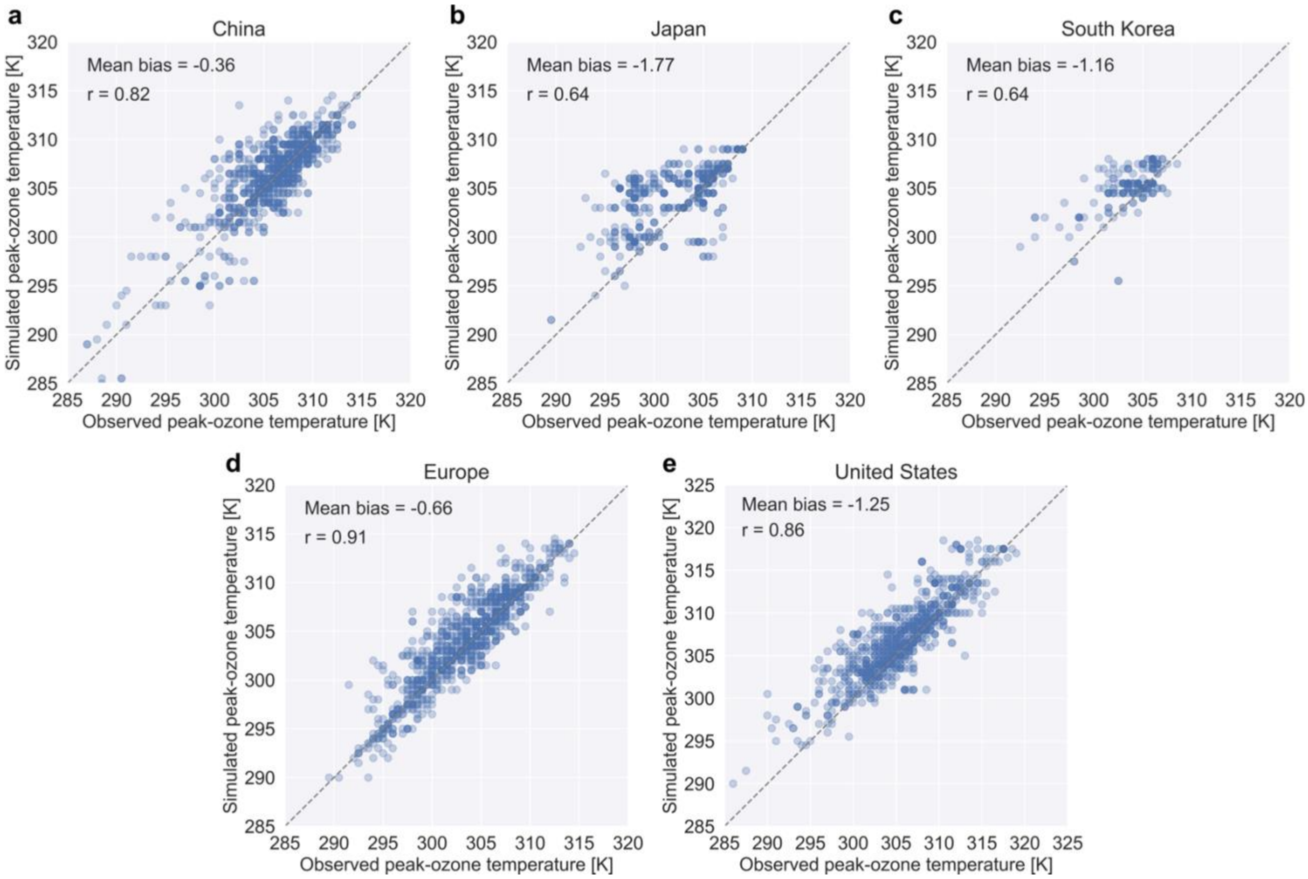

Supplementary Figure S6 | Comparison between observed (x-axis) and GEOS-Chem simulated (y-axis) peak-ozone temperatures over China, Japan, Korea, Europe, and the United States.

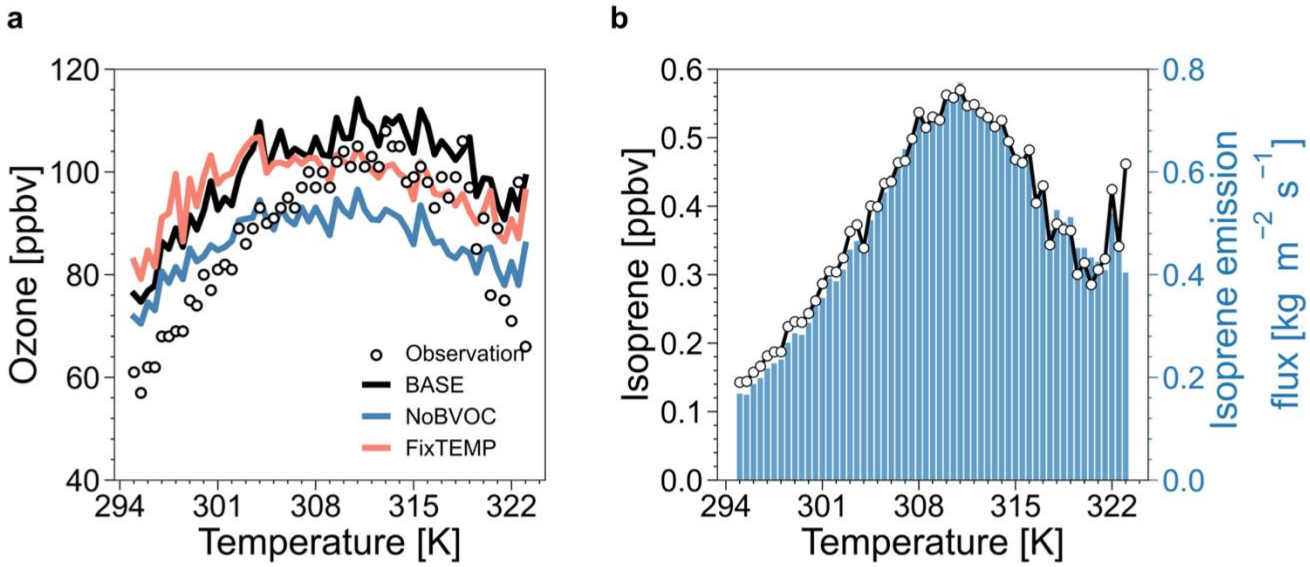

Supplementary Figure S7 | Ozone–temperature and isoprene–temperature relationships in the Southwest United States (California). (a) Same as Figure S4. (b) Response of simulated isoprene concentration (black lines) and emission fluxes (blue bars) with increased temperature.

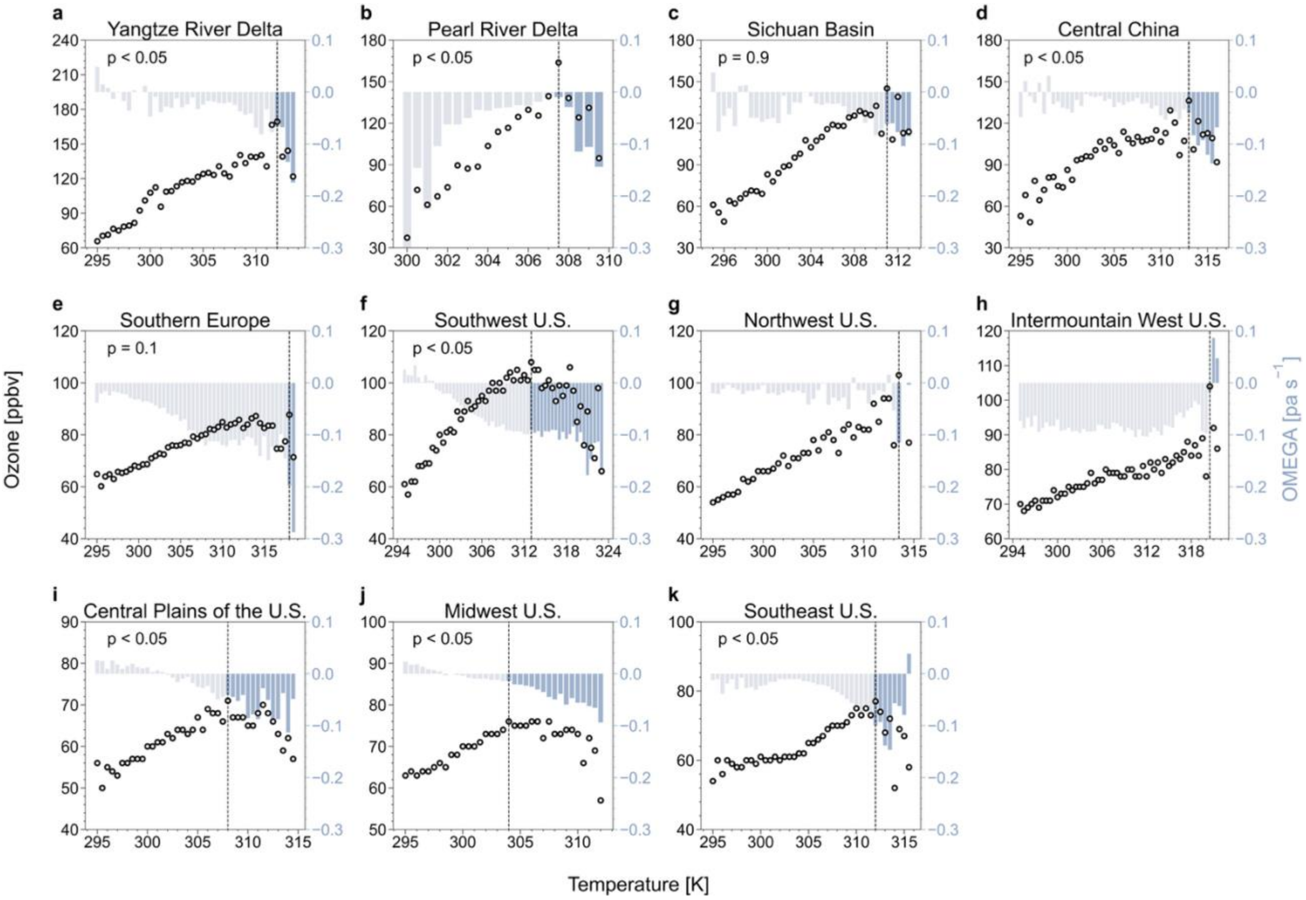

Supplementary Figure S8 | Same as Figure 2b but for key regions within China, Europe, and the United States.

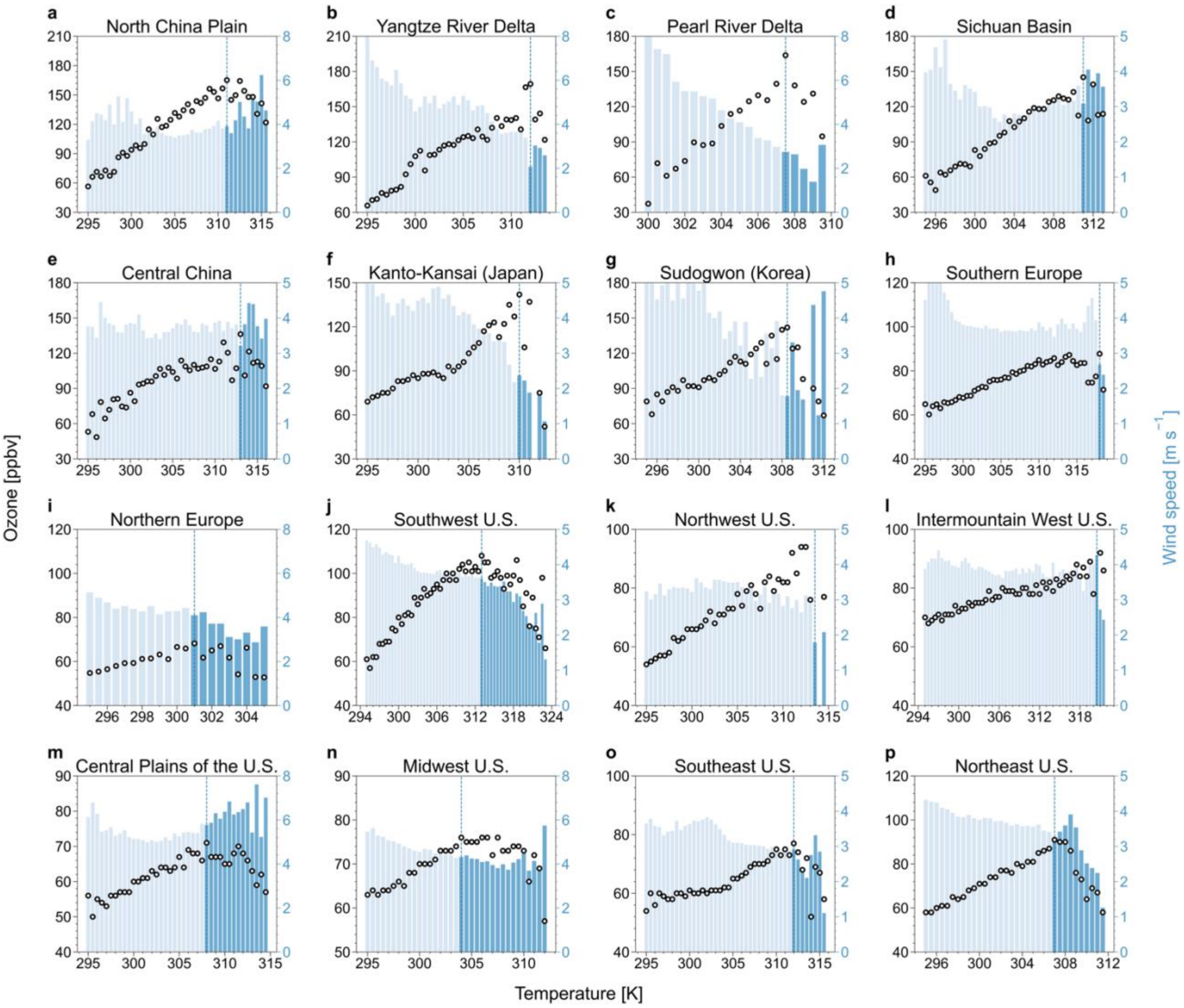

Supplementary Figure S9 | Same as Figure S8 but for surface wind speed.

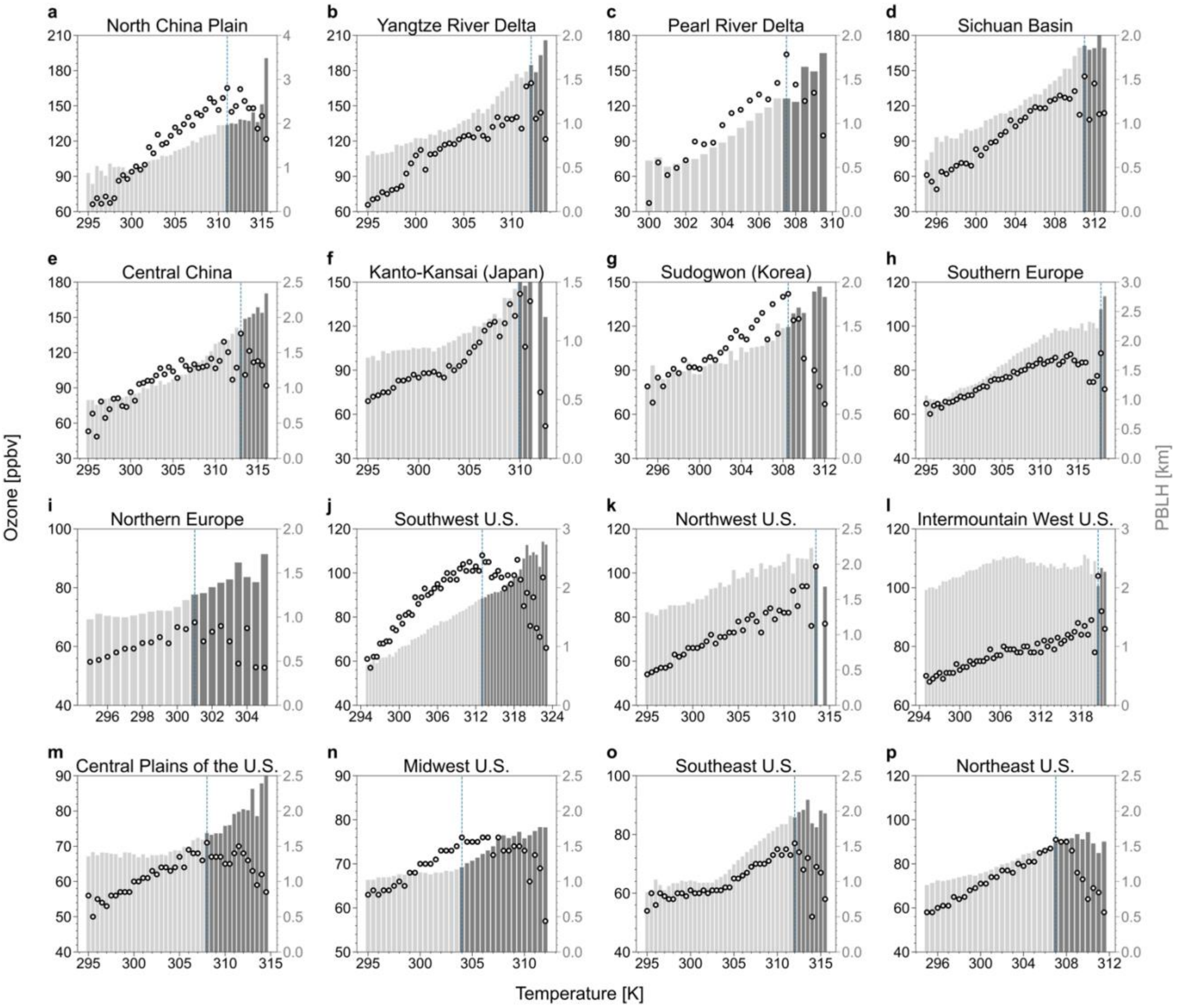

Supplementary Figure S10 | Same as Figure S8 but for Planetary Boundary Layer Height.

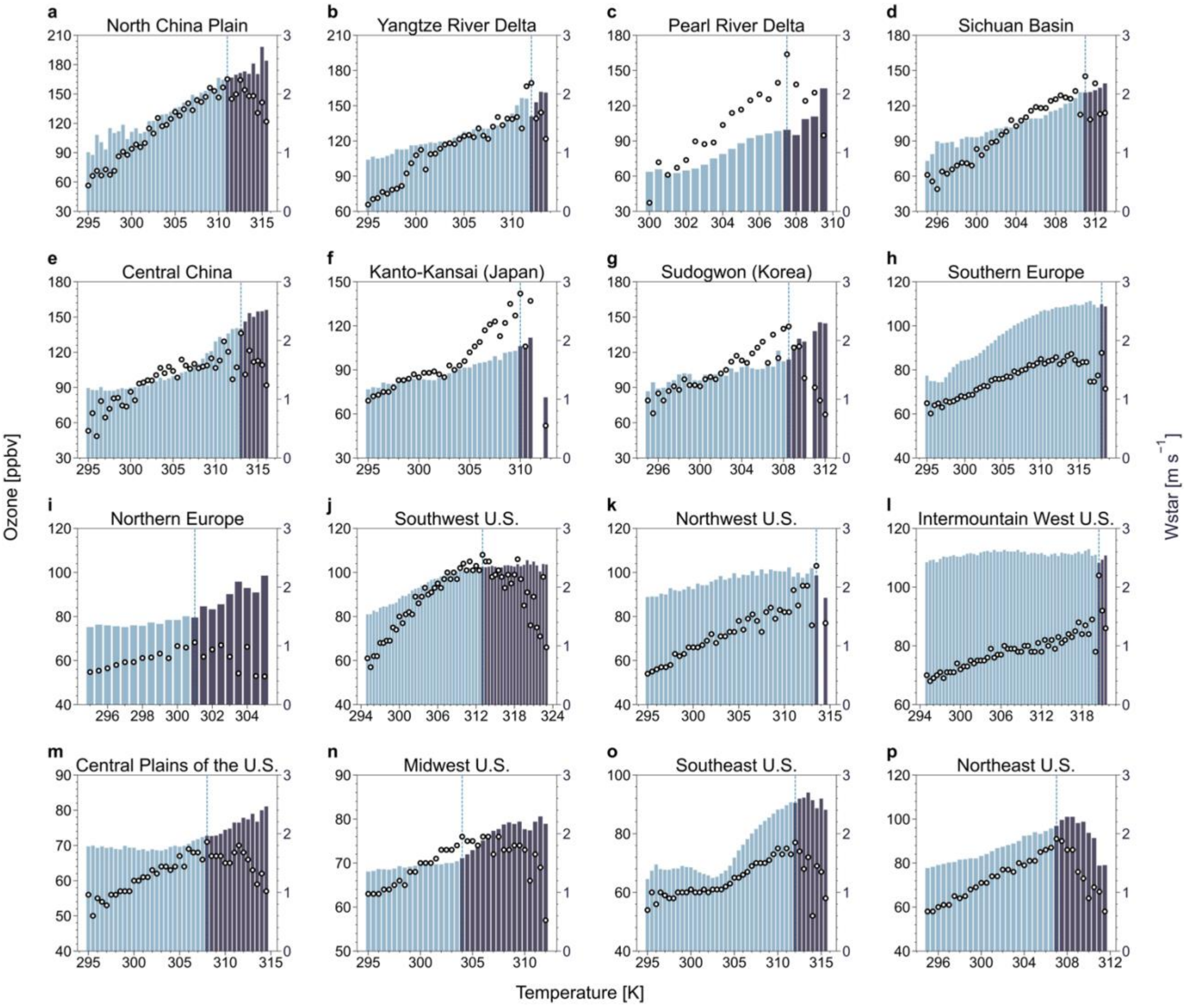

Supplementary Figure S11 | Same as Figure S8 but for convective velocity scale. The convective velocity scale is a characteristic velocity that represents the typical strength of buoyancy-driven turbulence in the convective boundary layer. The magnitude of this velocity scale mainly depends on the strength of surface heat flux and the depth of the boundary layer. It is defined as $w_* = \left(\frac{g}{\overline{T}} z_i (\overline{wT})_0\right)^{1/3}$, where $g/\overline{T}$ represents the buoyancy parameter for an ideal gas, z_i is the height of the convective layer (typically the height of the lowest inversion above the surface), and $(\overline{wT})_0$ denotes the surface kinematic heat flux, or the virtual temperature flux in a moist atmosphere[5,6].

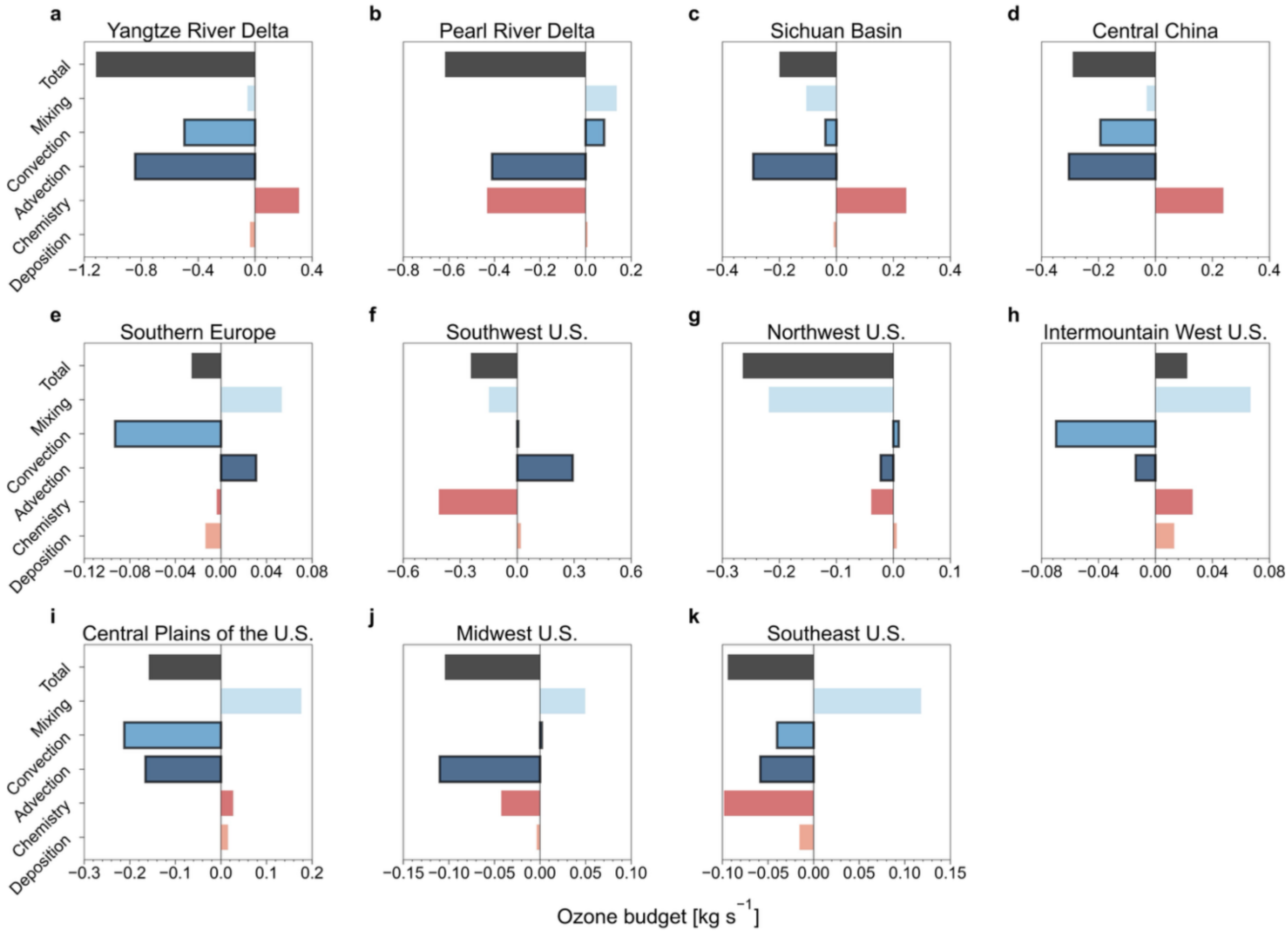

Supplementary Figure S12 | Same as Figure 2c but for key regions within China, Europe, and the United States.

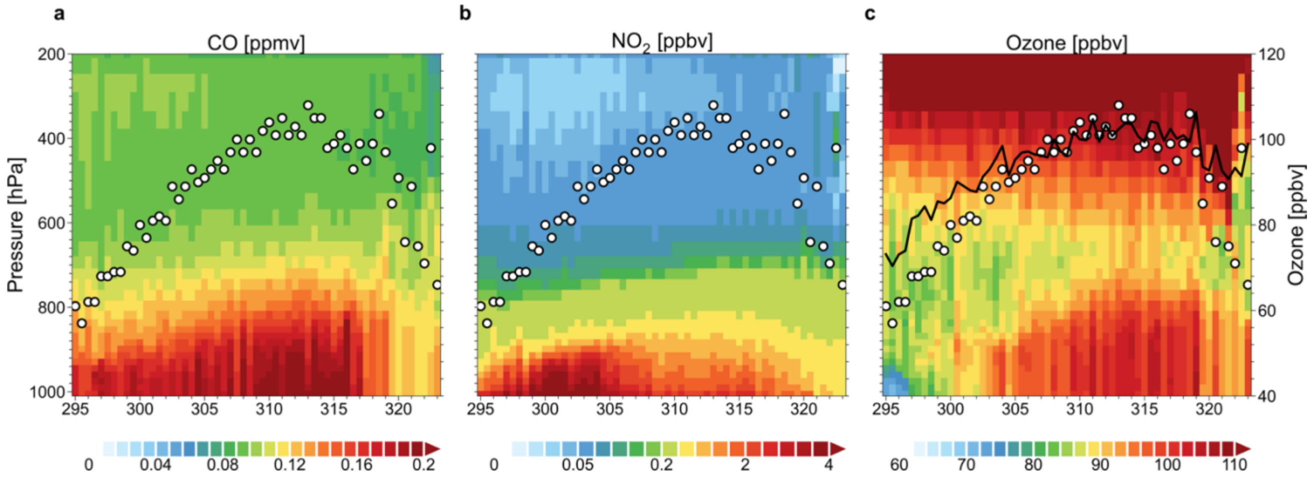

Supplementary Figure S13 | Temperature-dependent vertical profiles of CO, NO_2, and ozone over the Southwest U.S. Colors show the GEOS-Chem simulated CO (a), NO_2 (b), and ozone (c) as a function of pressure level and temperature. White circles indicate observed surface ozone concentrations binned by temperature. The black line in the right panel shows the simulated surface ozone–temperature relationship from the BASE simulation.

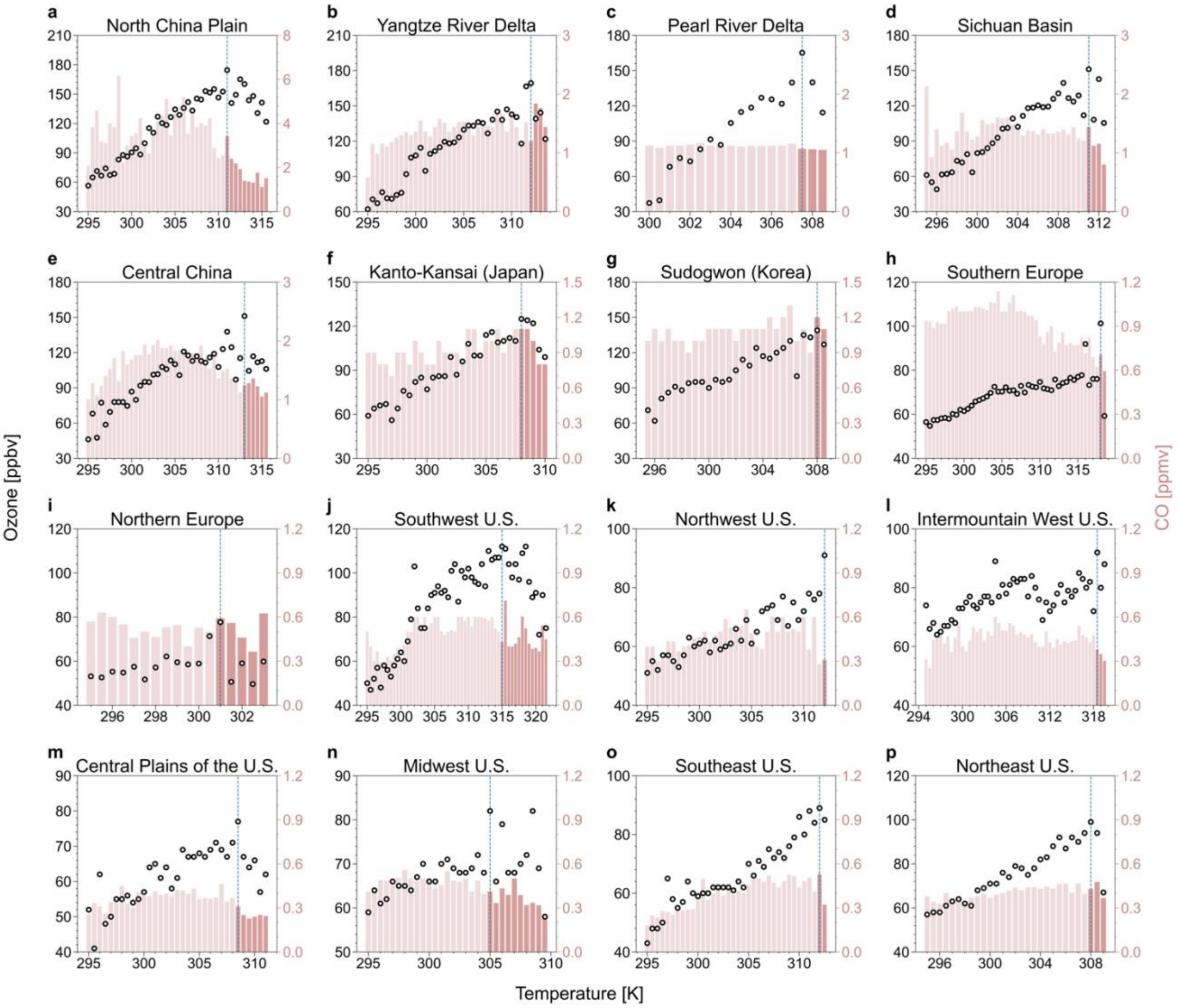

Supplementary Figure S14 | Same as Figure S8 but for CO concentrations. Results are averaged over sites with concurrent ozone and CO measurements that display ozone suppression.

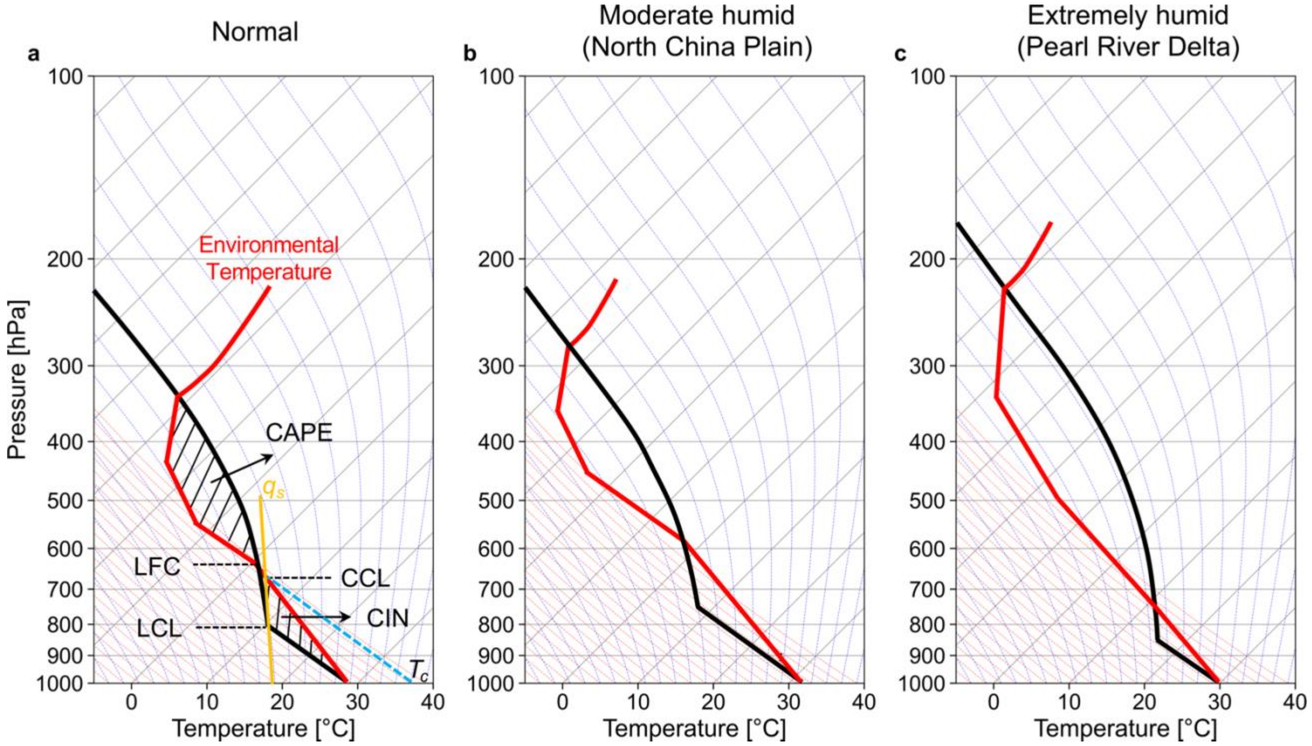

Supplementary Figure S15 | Conceptual Skew-T Log-P diagrams for three atmospheric states: (a) a "standard" diagram, (b) moderately moist conditions (RH~40-60%, such as the North China Plain), and (c) wet conditions. The red line represents the environmental temperature profile, while the black line indicates the temperature of an ascending air parcel following dry and wet adiabatic processes. The shaded regions illustrate the convective available potential energy and convective inhibition. The orange line indicates the saturation specific humidity.

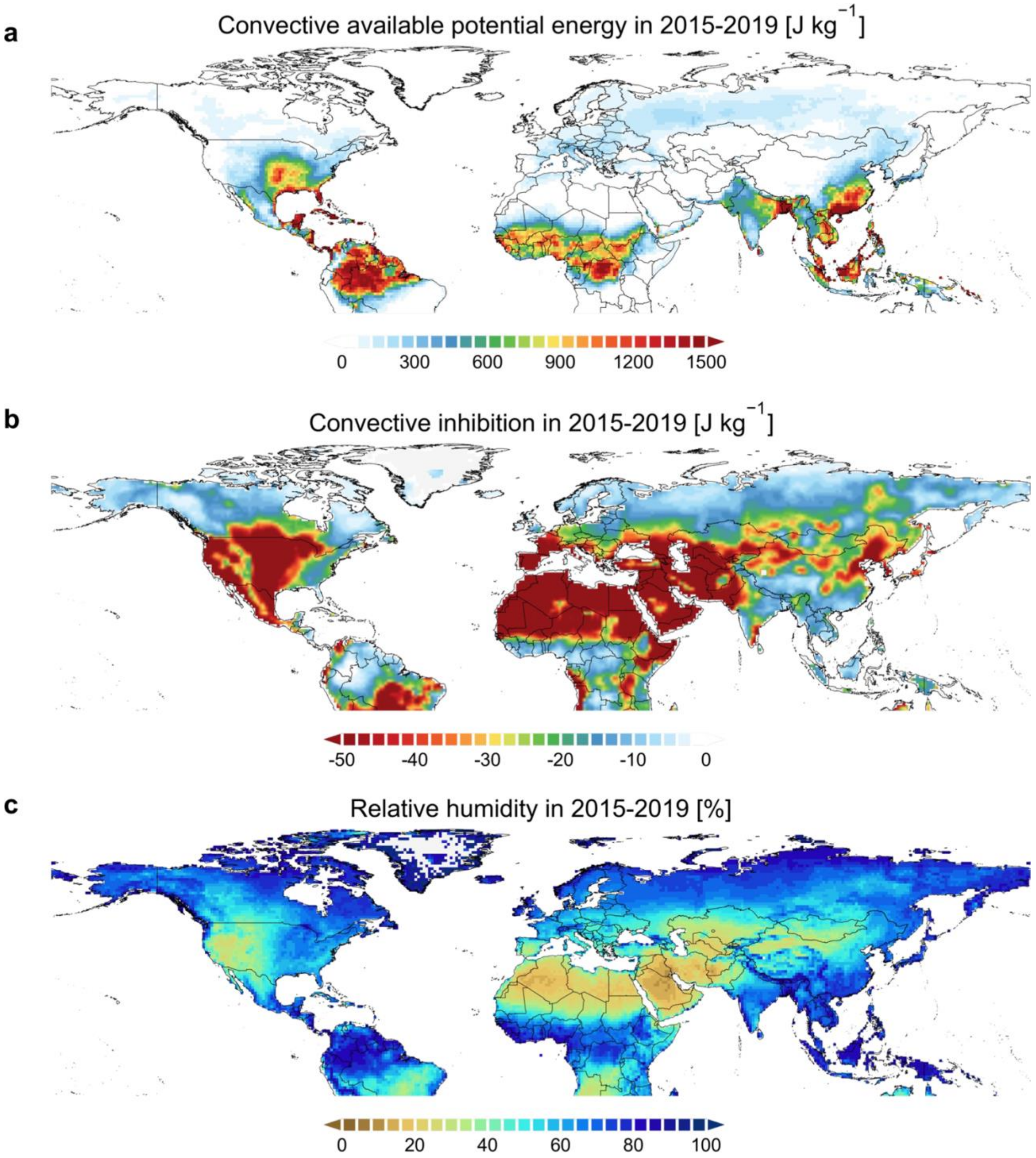

Supplementary Figure S16 | Spatial distribution of summertime (JJA) mean (a) convective available potential energy, (b) convective inhibition, and (c) relative humidity during 2015–2019.

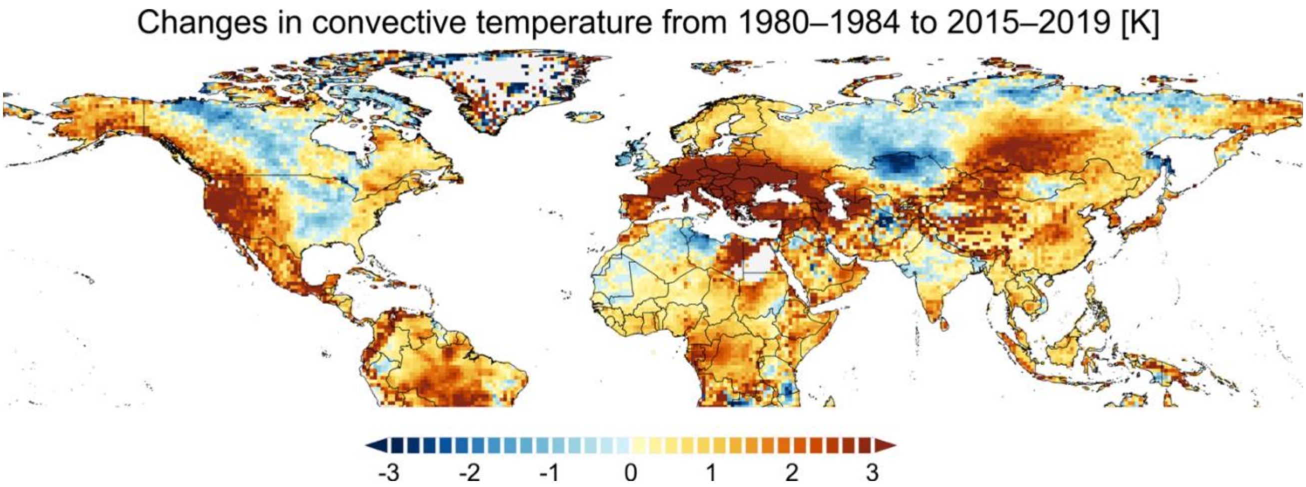

Changes in convective temperature from 1980–1984 to 2015–2019 [K]

Supplementary Figure S17 | Spatial distribution of summertime (JJA) changes in convective temperature (K) from 1980–1984 to 2015-2019.

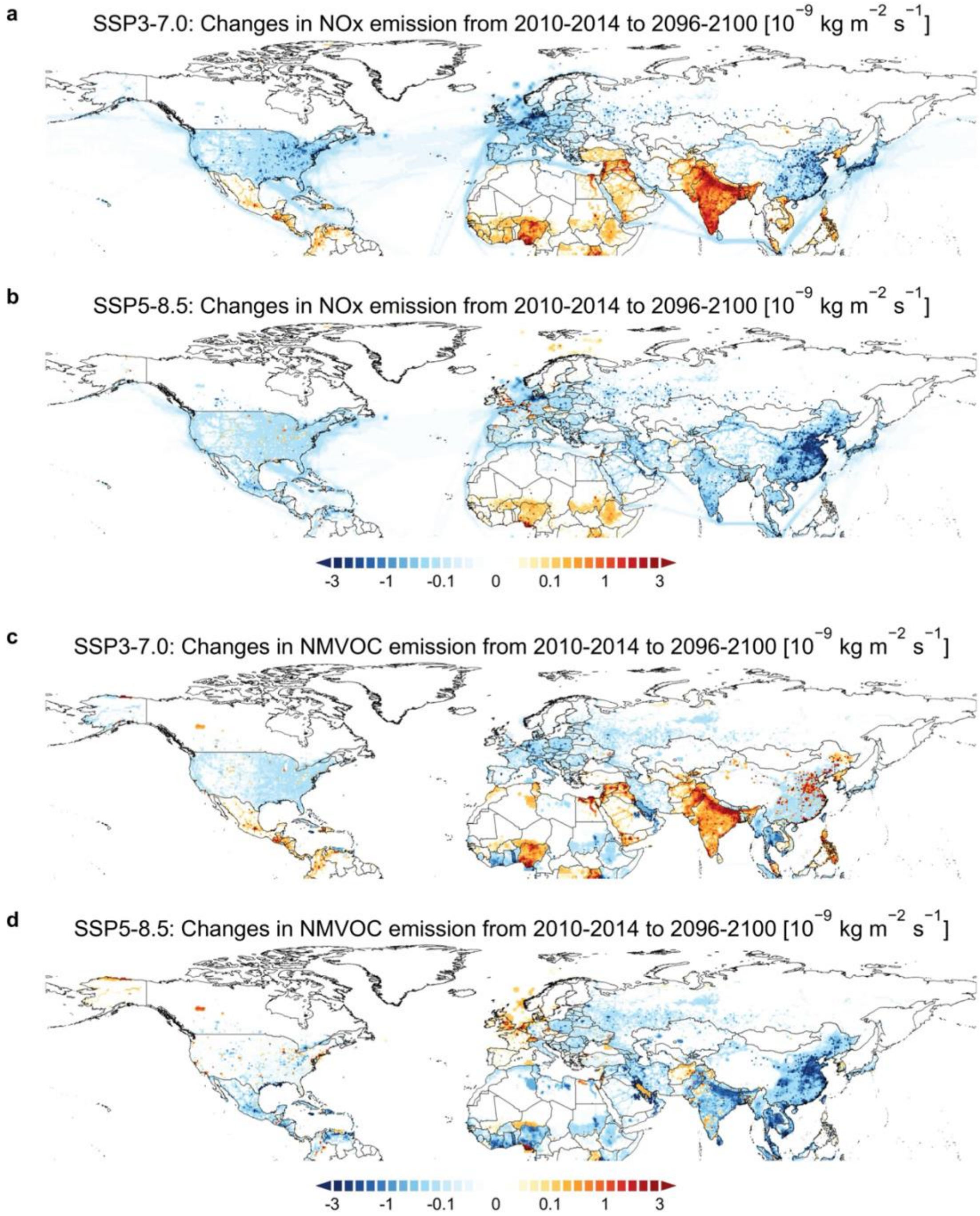

Supplementary Figure S18 | Spatial distribution of changes in (a,b) NO$_x$ emission and (c,d) NMVOCs emission from 2010-2014 to 2096–2100 under the SSP3-7.0 and SSP5-8.5.

Supplementary Table S1 | Information of hourly observations collected by individual national monitoring networks.

Country	Number of ozone sites	Number of CO sites	Source agent	Source URLs
China	2028	2028	China National Environmental Monitoring Center	http://106.37.208.233:20035/
South Korea	554	593	Korean Ministry of Environment	https://airkorea.or.kr/
Japan	899	61	National Institute for Environmental Studies	https://tenbou.nies.go.jp/download/
United States	1681	426	Environmental Protection Agency Air Quality System monitoring network	https://aqs.epa.gov/aqsweb/airdata/download_files.html
Europe	2240	1609	European Environment Agency	https://eeadmz1-downloads-webapp.azurewebsites.net/

Supplementary Table S2 | Configurations of model simulations.

Cases	Meteorology	Anthropogenic emissions	BVOC emissions
BASE	2015-2019	2015-2019	On
FixTEMP	2015-2019 (with a normalized temperature field in the model)	2015-2019	On
NoBVOC	2015-2019	2015-2019	Off
AEMI30%OFF	2015-2019	2015-2019 (with 30% reduction in anthropogenic NO_x and VOCs emissions)	On
1980MET	1980-1984	2015-2019	On

Supplementary Table S3 | List of CMIP6 models analyzed in this study.

No.	Name of models	Frequency	Var	Member			Countries	Spatial Resolution
				Historical	SSP3-7.0	SSP5-8.5		
1	BCC-CSM2-MR	6hr	ta / hus	√	/	√	China	160 × 320
2	MIROC6	6hr	ta / hus	√	/	√	Japan	128 × 256
3	MPI-ESM1-2-LR	6hr	ta / hus	√	/	√	Germany	96 × 192
4	MRI-ESM2-0	6hr	ta / hus	√	/	√	Japan	160 × 320
5	NorESM2-LM	6hr	ta / hus	√	/	√	Norway	96 × 144
6	GFDL-ESM4	1hr	sfo3 / tas	√	√	√	USA	180 × 288

References

1. Wang, H. *et al.* Deciphering decadal urban ozone trends from historical records since 1980. *Natl. Sci. Rev.* **11**, (2024).
2. Steiner, A. L. *et al.* Observed suppression of ozone formation at extremely high temperatures due to chemical and biophysical feedbacks. *Proc. Natl. Acad. Sci. USA* **107**, 19685-19690, (2010).
3. Shen, L., Mickley, L. J. & Gilleland, E. Impact of increasing heat waves on U.S. ozone episodes in the 2050s: Results from a multimodel analysis using extreme value theory. *Geophys. Res. Lett.* **43**, 4017-4025, (2016).
4. Ning, G., Wardle, D. A. & Yim, S. H. L. Suppression of Ozone Formation at High Temperature in China: From Historical Observations to Future Projections. *Geophys. Res. Lett.* **49**, e2021GL097090, (2022).
5. Fan, Y., Li, Y., Wang, X. & Catalano, F. A New Convective Velocity Scale for Studying Diurnal Urban Heat Island Circulation. *J. Appl. Meteor. Climatol.* **55**, 2151-2164, (2016).
6. Deardorff, J. W. Convective Velocity and Temperature Scales for the Unstable Planetary Boundary Layer and for Rayleigh Convection. *J. Atmos. Sci.* **27**, 1211-1213, (1970).